Journal Pre-proofs

Field-Scale Soil Moisture Estimation Using Sentinel-1 GRD SAR Data

Narayanarao Bhogapurapu, Subhadip Dey, Saeid Homayouni, Avik Bhattacharya, Y.S. Rao

PII: S0273-1177(22)00205-8
DOI: https://doi.org/10.1016/j.asr.2022.03.019
Reference: JASR 15811

To appear in: *Advances in Space Research*

Received Date: 31 October 2021
Revised Date: 14 March 2022
Accepted Date: 19 March 2022

Please cite this article as: Bhogapurapu, N., Dey, S., Homayouni, S., Bhattacharya, A., Rao, Y.S., Field-Scale Soil Moisture Estimation Using Sentinel-1 GRD SAR Data, *Advances in Space Research* (2022), doi: https://doi.org/10.1016/j.asr.2022.03.019

Highlights

- Proposed an extended change detection methodology for soil moisture retrieval of croplands using Dual-pol Radar Vegetation Index for GRD data, $DpRVI_c$.
- $DpRVI_c$ outperforms NDVI for soil moisture estimation over croplands and shrublands.

Field-Scale Soil Moisture Estimation Using Sentinel-1 GRD SAR Data

Narayanarao Bhogapurapu[a,*], Subhadip Dey[a], Saeid Homayouni[b], Avik Bhattacharya[a], Y. S. Rao[a]

[a] *Microwave Remote Sensing Lab, Centre of Studies in Resources Engineering, Indian Institute of Technology Bombay, Mumbai 400076, India*
[b] *Centre Eau Terre Environnement, Institut National de la Recherche Scientifique, 490 rue de la Couronne Street, Quebec G1K 9A9, Canada*

Abstract

Soil moisture is a critical land variable that controls the energy and mass balance in land-atmosphere interactions. Spaceborne Synthetic Aperture Radar (SAR) sensors offer an efficient way to map and monitor soil moisture because of their sensitivity towards the dielectric and geometric properties of the target. In addition, SAR acquisitions are weather-independent, providing a significant advantage over optical imaging during periods of cloud cover. However, vegetation cover makes these processes more complex and influences the interaction of SAR backscatter resulting from combined soil matrix and vegetation cover. Therefore, using SAR data, it is necessary to compensate for vegetation contribution in total backscatter while estimating soil moisture over the vegetated soil surface. This study presents a technique that utilizes a vegetation index derived from SAR data to generate high-resolution soil moisture maps. It is noteworthy that this proposed soil

*Corresponding author: Narayanarao Bhogapurapu (narayanarao.bhogapurapu@gmail.com)

moisture retrieval method uses only the dual-polarimetric Ground Range Detected (GRD) SAR product, i.e., only backscatter intensities. Hence, the proposed method has a high potential for operational soil moisture monitoring globally. We validated over 34 soil moisture stations of the Texas Soil Observation Network (TxSON) using time-series Sentinel-1 SAR data. The Root Mean Square Error (RMSE) values for estimated volumetric soil moisture are within the range of $0.048\,\mathrm{m^3\,m^{-3}}$ to $0.055\,\mathrm{m^3\,m^{-3}}$ with the Pearson correlation coefficient $r > 0.79$.

Keywords: Soil moisture, DpRVI_c, NDVI, change detection, Sentinel-1

1. Introduction

Soil moisture is a critical land variable that controls the energy and mass balance in land-atmosphere interactions (Pauwels and De Lannoy, 2006; Seneviratne et al., 2010; Karthikeyan et al., 2017). Soil moisture has a wide range of applications including weather forecasting (Scipal et al., 2008), flood prediction (Wanders et al., 2014; Massari et al., 2018), drought monitoring (Mishra et al., 2017; Martínez-Fernández et al., 2016) and crop modelling (Ines et al., 2013). Specifically to the agriculture sector, the highly dynamic nature (spatial and temporal) of surface soil moisture affects crop productivity, particularly at critical plant development stages (Champagne et al., 2012; Karthikeyan et al., 2020). Remote sensing techniques offer many advantages over conventional methods for monitoring soils and crops. In particular, Synthetic Aperture Radar (SAR) data have been effectively used in estimating soil moisture at high spatio-temporal resolutions (Shi et al., 1997; Hornacek et al., 2012; Bauer-Marschallinger et al., 2018).

The sensitivity of SAR response to dielectric and geometrical properties of a target is observed by several investigators using ground, aircraft, and spaceborne platforms. For land targets, the intensity and scattering angular behavior of SAR responses are impacted by the volume of water in the soil, the micro and macro roughness of the surface roughness, and the characteristics of the vegetation cover (Ulaby, 1982; Karthikeyan et al., 2017). Typically for bare soil conditions, backscatter intensity is linearly related to volumetric soil moisture (Ulaby, 1974; Ulaby et al., 1978; Dubois et al., 1995; Baghdadi et al., 2006). Inversion of surface scattering models such as Integral Equation Model (IEM) Fung et al. (1992), and empirical models developed by Oh et al. (1992); Dubois et al. (1995) can be utilized to estimate soil moisture within the validity range of each model. These models were developed for bare soils, and as such, the use of these models to estimate soil moisture under vegetated conditions yields high soil moisture uncertainties (Oh et al., 1992; Jagdhuber et al., 2012).

The initial step in estimating soil moisture in the presence of vegetation is to separate the contributions to the SAR response from the vegetation and the soil. If they are separated successfully, the soil contributions can be used to invert scattering or empirical soil moisture models. However, the uncertainties in soil moisture estimations develop with the increasing complexity of the structure and dielectric properties of vegetation cover (Oh et al., 1992; Millard and Richardson, 2018). The methods of estimating soil moisture under vegetation cover can be primarily categorized into five groups: coupling the surface scattering models with vegetation models (Baghdadi et al., 2015; Bao et al., 2018; El Hajj et al., 2017; Attarzadeh et al., 2018; Ma et al., 2020) (also called synergetic approaches), scattering power decomposition (Hajnsek et al., 2009; Jagdhuber et al., 2012), change detection approaches (Wagner et al., 1999; Ouellette et al., 2017; Bauer-Marschallinger et al., 2018), physical model-based data driven methods like artificial neural networks (Paloscia et al., 2013) and data cube approaches (Kim et al., 2013).

Change detection-based approaches of soil moisture estimation are one of the popular techniques to generate global high-resolution soil moisture products (Bauer-Marschallinger et al., 2018; Balenzano et al., 2021). (Wagner et al., 1999) introduced the change detection technique to estimate soil moisture from scatterometer data. Later Zribi et al. (2008) used NDVI to correct the vegetation effect on soil backscatter. Balenzano et al. (2010) introduced another change detection approach using backscatter ratios of consecutive acquisitions from dense temporal multi-frequency airborne SAR data. Recently, the change detection approach proposed by Wagner et al. (1999) has been modified according to Sentinel-1 SAR data characteristics by Bauer-Marschallinger et al. (2018). Further, Gao et al. (2017) adapted the change detection approach for Sentinel-1 data and utilized NDVI from Sentinel-2 data for vegetation correction while estimating soil moisture over vegetation-covered soils.

Although optical remote sensing-derived products show significant promise in estimating soil moisture, these data collections are limited to cloud-free conditions. The interference of clouds in image acquisitions is particularly problematic for operational retrievals, implemented at regional scales. Notably, crop development is very dynamic during the monsoon period when the likelihood of clouds is high. These cloudy conditions impose a challenge in collecting spectral signatures for major crops, such as rice and sugarcane. Hence, during critical periods of crop development, SAR-derived vegetation descriptors could be a valuable alternative to optical remote sensing-derived products.

Other major limitations of optical derived indices include the saturation of spectral signatures for dense crop foliage (Asrar et al., 1984; Hatfield et al., 1985; Sellers, 1985). For example, NDVI becomes insensitive to high values of leaf area index (Hobbs, 1995; Asner et al., 2003; Chen et al., 2006). These multi-spectral indices respond to plant chlorophyll content, parenchyma tissue arrangements, and photosynthetic potentials of vegetation. After a certain period of crop phenological development, the changes in these vegetation components become negligible. Consequently, optical vegetation indices also become insensitive to future vegetation development, even though significant differences in crop geometry and biomass continue. One could exploit SAR responses to capture the continued growth of the canopy, considering the sensitivity of backscatter to crop structure and biophysical characteristics.

In this regard, SAR derived descriptors have been successfully utilized in vegetation monitoring (Dey et al., 2020a,c, 2021a,b) and soil moisture studies (Bhogapurapu et al., 2020a,b, 2021b). Several vegetation descriptors such as the Radar Vegetation Index (RVI) for dual-pol (Trudel et al., 2012), Dual-Pol SAR Vegetation Index (DPSVI) (Periasamy, 2018), and Dual-pol Radar Vegetation Index (DpRVI) (Mandal et al., 2020; Bhogapurapu et al., 2022) have been developed for crop growth monitoring and biophysical parameter retrieval (Dey et al., 2020b). It is evident from these studies that SAR-derived vegetation descriptors are an effective way to monitor and quantify vegetation at the different phenological windows. However, previous studies did not explore using change detection-based methods to utilize SAR-derived vegetation descriptors for soil moisture estimation.

This study utilizes a SAR-derived vegetation index (DpRVI_c) that exploits the available polarimetric information in dual-pol GRD SAR data. The formalism of the index jointly uses the co-pol purity parameter and normalized co-pol intensity parameter. The co-pol purity parameter infers the mix of two polarization intensities within a pixel. The proportion of this mix relates to the amount of randomness in the scattering, relating it to vegetation quantity. Besides, the normalized co-pol intensity parameter represents the dominant pseudo probability for dual-pol SAR data. We use this index in a change detection-based approach to estimate surface soil moisture over croplands and shrublands.

The manuscript unveils as follows. Section 2 details the study area and dataset used in this study. This is followed by a methodology section (Section 3) about the proposed adaption of the soil moisture retrieval algorithm for SAR-based vegetation indices. Subsequently, results from an evaluation of the obtained $100\,\mathrm{m}\times100\,\mathrm{m}$ Sentinel-1 soil moisture data over Texas in the United States are presented and discussed in Section 4. The conclusions emphasize the research aspects and provide impressions of the possible future scope of the proposed algorithm.

2. Study area and datasets

We used the ground truth soil moisture data from the Texas Soil Observation Network (TxSON) in this study. The TxSON area is an intensively monitored area ($1300\,\mathrm{km}^2$) located near Fredericksburg, Texas. This dense network consists of 40 in-situ locations nested at 36, 9, and 3 km within the Equal-Area Scalable Earth Grid and serves as a Core Calibration and Validation Site for NASA's Soil Moisture Active Passive mission (Caldwell et al., 2019). Soil moisture measurements from the top 0 cm to 5 cm are used in this study. Soil texture across the stations varies from sand to silty loam. Major land cover classes present in the network are shrublands, croplands, and evergreen forests. In this study, we have used in-situ data acquired majorly over croplands and shrublands. Croplands majorly consists of viticulture and pastures, whereas vegetation in the shrublands includes woody plants (Ashe juniper and honey mesquite) and a mixture of short and mid-height grasses (grama, switchgrass, bluestem, curlymesquite) (Caldwell et al., 2019).

Soil moisture data from 34 stations, including 27 stations from shrublands and seven stations from croplands, is processed and used in this study. A map representing the extent of the study area and locations of the TxSON stations is shown in Figure 1. Further details on the TxSON study site can be found in Caldwell et al. (2019).

Sentinel-1 (S1) dual polarimetric SAR data acquired from March 2015 to August 2019, a total of 90 scenes are used in this study. The S1 data is acquired in Interferometric Wide Swath mode (IW) with an incidence angle range of 33.67° to 36.19° across the study area. The S1 GRD data is despeckled using a 5×5 boxcar filter and further resampled to 100 m. Subsequently, the Dual-pol Radar Vegetation Index for GRD SAR data was generated using PolSAR tools plugin (Bhogapurapu et al., 2021c). We have used NDVI derived from Moderate Resolution Imaging Spectroradiometer

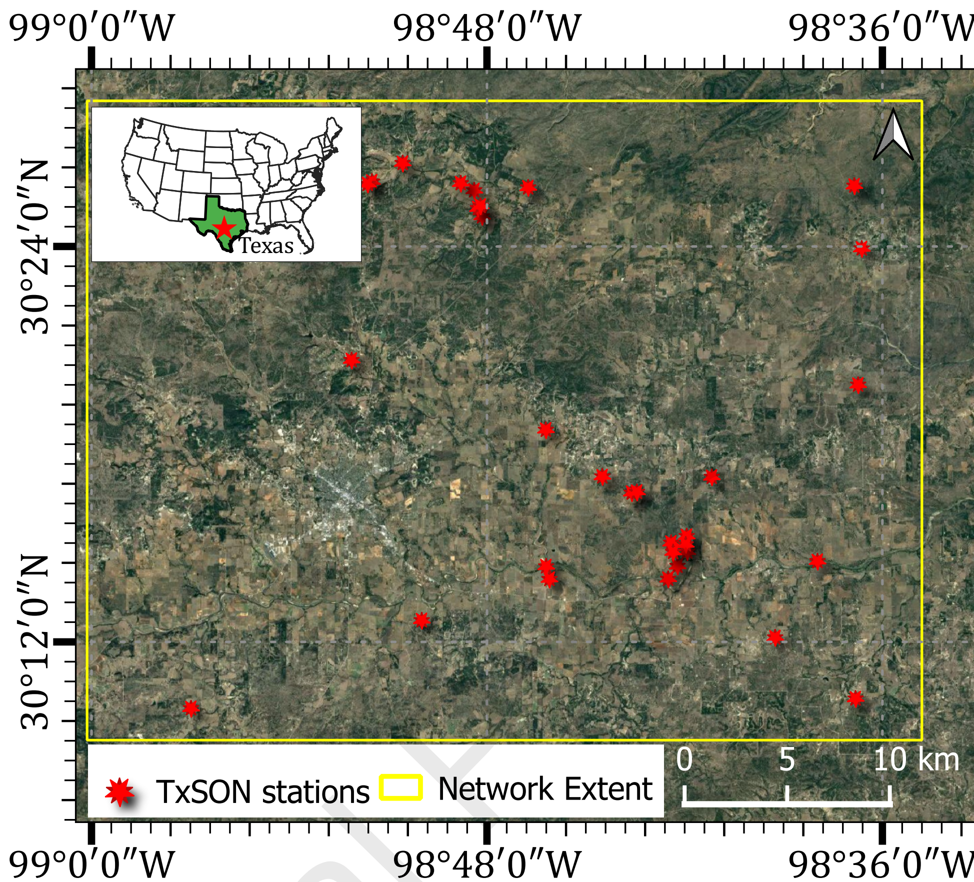

Figure 1: Map of study area showing the locations of the soil moisture stations of Texas Soil Observation Network.

(MODIS) Terra Surface Reflectance 8-Day Global 250 m (MOD09Q1.006) available in Google Earth Engine (GEE).

3. Methodology

This section proposes a modified change detection approach to estimate soil moisture using dual polarimetric SAR data. We extend the method proposed by Zribi et al. (2008) to estimate soil moisture. We utilize the vegetation index derived from dual-pol SAR datasets to correct the vegetation effect on soil backscatter. Furthermore, we also use NDVI derived from optical data to compensate for vegetation attenuation on soil backscatter for a comparative study.

3.1. Vegetation Indices

NDVI has been widely used to retrieve crop biophysical parameters such as LAI (Liu et al., 2012) and biomass (Mutanga and Skidmore, 2004). Besides, it has been used to compensate for vegetation effects on soil backscatter when retrieving soil moisture (Bao et al., 2018; Li and Wang, 2018). From Rousel et al. (1973), NDVI can be derived from optical remote sensing data, as shown in Eq. (1).

$$\mathrm{NDVI} = \frac{\rho_{\mathrm{NIR}} - \rho_{\mathrm{R}}}{\rho_{\mathrm{NIR}} + \rho_{\mathrm{R}}} \tag{1}$$

where, ρ_{NIR} is spectral reflectance in the near-infrared wavelength region (band-1 of MODIS (620-670 nm)) and ρ_{R} is spectral reflectance in red wavelength region (band-2 of MODIS (841-876 nm)).

In dual cross-polarimetric GRD SAR data product, we obtain backscatter response either in $(\sigma^\circ_{\mathrm{VV}}, \sigma^\circ_{\mathrm{VH}})_{\mathrm{dB}}$ or $(\sigma^\circ_{\mathrm{HH}}, \sigma^\circ_{\mathrm{HV}})_{\mathrm{dB}}$[1] modes. In general, for a mono-static antenna configuration and a natural scene, we assume $\sigma^\circ_{\mathrm{XY}} \leq \sigma^\circ_{\mathrm{XX}}$ (where X and Y are H or V polarizations respectively) (Cloude, 2009). Using this assumption, we consider a ratio parameter, $0 \leq q = \dfrac{\sigma^\circ_{\mathrm{XY}}}{\sigma^\circ_{\mathrm{XX}}} \leq 1$, in the linear scale. This parameter has been widely used in the literature as

[1] Here, H and V are the horizontal and vertical transmit and received polarization components. The subscript dB represents the GRD SAR data products in decibel (dB) scale.

a descriptor for several crop monitoring applications (Della Vecchia et al., 2008; Vreugdenhil et al., 2018; Homayouni et al., 2019). On the other hand, vegetation indices in the form of the ratio of backscatter intensities have proven to be effective to characterize vegetation morphology.

Using the backscatter intensity ratio q, we define the co-pol purity parameter m_c given in Eq. (2). The co-pol return will be high in low vegetation conditions, where the cross-pol return is negligible ($q \to 0$). From Eq. (2), one can immediately observe that m_c is high for bare field conditions, while it gradually decreases with an increase in vegetation density.

$$m_c = \frac{1-q}{1+q}, \qquad 0 \leq m_c \leq 1 \tag{2}$$

Therefore, one can conclude that the m_c parameter infers the mix of two polarization intensities in a pixel and thus indicates the purity of the co-pol component within the same pixel. It can be noted that for $q = 1$, $m_c = 0$, and for $q = 0$, $m_c = 1$. In between these two extreme cases, $1 > q > 0$, $0 < m_c < 1$. Besides, we also define the normalized co-pol intensity parameter (β_c) as,

$$\beta_c = \frac{1}{1+q}, \qquad 0.5 \leq \beta_c \leq 1 \tag{3}$$

The co-pol purity parameter m_c is multiplied with the normalized co-pol intensity parameter β_c, representing the dominant pseudo probability for dual-pol SAR data. The product of m_c and β_c then characterizes the overall purity of the co-pol component. We then obtain a measure of scattering randomness by subtracting the product of m_c and β_c from unity, as given in

Eq. (4). The variation in the measure of this scattering randomness could be attributed to vegetation canopy development at different phenology stages.

For example, in the case of sparse vegetation conditions, the scattering from the soil surface is usually dominant. However, as the density of vegetation increases, multiple scattering from the canopy and soil is more apparent. Hence, one can expect m_c to decrease with the increase in vegetation canopy density. A similar sensitivity of the co-pol purity parameter is also highlighted with increasing target morphological complexity (Mandal et al., 2020; Bhogapurapu et al., 2021a, 2022).

$$\begin{aligned} \mathrm{DpRVI}_c &= 1 - m_c\beta_c \\ &= \frac{q(q+3)}{(q+1)^2}, \qquad 0 \leq \mathrm{DpRVI}_c \leq 1 \end{aligned} \tag{4}$$

Therefore, from Eq. 4, it is clear that DpRVI_c essentially indicate the impure fraction of the co-pol component in the scattered wave. For example, in the case of pure or point target scattering with a dominant scattering probability, $\beta_c = 1$ and $m_c = 1$. This state corresponds to $\mathrm{DpRVI}_c = 0$. Theoretically, for a smooth bare surface (i.e., Bragg scattering), $\sigma^\circ_{\mathrm{XX}} \gg \sigma^\circ_{\mathrm{XY}}$, with a high value of m_c. In the case of completely random scattering, $m_c = 0$ and $\beta_c = 0.5$. This suggests that $\sigma^\circ_{\mathrm{XY}} = \sigma^\circ_{\mathrm{XX}}$ for which $\mathrm{DpRVI}_c = 1$. For natural targets like fully developed vegetation canopies, $m_c \approx 0$ and $\beta_c \approx 0.5$, leading to higher DpRVI_c, i.e., $\mathrm{DpRVI}_c \approx 1$.

3.2. Soil moisture Estimation

We use a change detection approach accompanied by vegetation correction to estimate soil moisture over shrublands and croplands. This approach was initially proposed by (Zribi et al., 2008) for scatterometer data while using NDVI to correct for vegetation influence. In this study, we adapted this approach for Sentinel-1 observations. The inversion algorithm is optimized to take advantage of the dense temporal data. The total backscatter from the surface can be expressed as the sum of the contributions from soil and vegetation, attenuated by it as,

$$\sigma^\circ_{\mathrm{total}} = \sigma^\circ_{\mathrm{veg}} + \delta^2(\phi)\,\sigma^\circ_{\mathrm{soil}} \tag{5}$$

where $\delta^2(\phi) = \exp\left[-2\tau/\cos\phi\right]$ is the two-way attenuation factor, ϕ is the incidence angle, and τ is the optical thickness parameter that depends on the vegetation water content and geometry of the vegetation canopy.

One can potentially monitor any temporal evolution of the soil moisture by detecting changes in the backscattered signal. If we consider radar signals scattered from the same cell, one could eliminate roughness effects and certain vegetation effects by computing the difference between the data recorded at different dates. This approach assumes that the change in backscattered signal is only due to local variations in soil moisture.

First we calculate the historical minimum backscatter value ($\sigma^\circ_{\mathrm{dry}}$) excluding 2 % on either sides of historical data distribution for a given pixel. Now, considering that $\sigma^\circ_{\mathrm{dry}}$ corresponds to the driest soil state for the given pixel, we calculate the change in backscatter $\Delta\sigma$ as,

$$\Delta\sigma = \sigma^\circ_{\mathrm{dB}} - \sigma^\circ_{\mathrm{dry}} = f(\mathrm{veg}, \Theta) \tag{6}$$

where, $\Delta\sigma$ is a function of vegetation and soil moisture Θ. One can conceptually realize the relation between $\Delta\sigma$, soil moisture, and vegetation as shown in Figure 2. The X-axis depicts the vegetation index, and the Y-axis indicates the change in backscatter, $\Delta\sigma$. The red line is the dry reference. The upper bound is the wet reference (represented with a blue dashed line). The shaded region is the observed $\Delta\sigma$ values for various vegetation conditions.

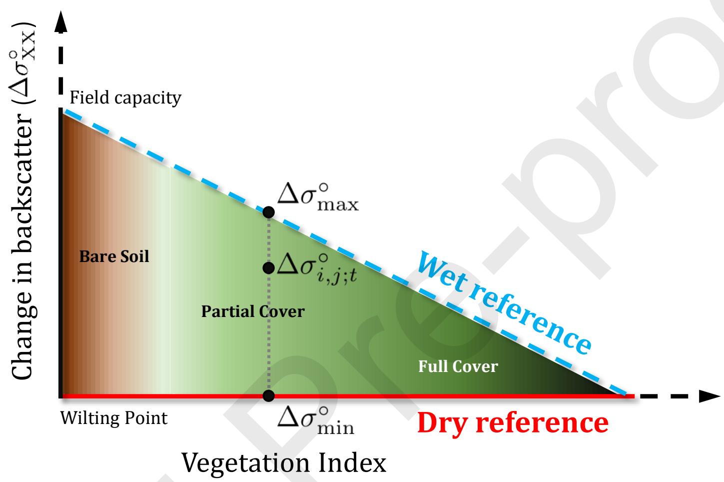

Figure 2: Conceptual diagram of change in backscatter ($\Delta\sigma^{\circ}_{\mathrm{XX}}$) and vegetation index space.

We can observe that the overall dynamic range of $\Delta\sigma$ decreases with an increase in vegetation cover/density. This decrease in the dynamic range indicates a decreased sensitivity of $\Delta\sigma$ to the change in soil moisture, which is also reported in previous studies (Zribi et al., 2008; Gao et al., 2017). However, the slope and shape of the upper bound (i.e., the wet reference) is a function of the vegetation index. In this regard, Zribi et al. (2008) used a quadratic function of NDVI, whereas Gao et al. (2017) used a linear function of NDVI to represent the wet reference.

Now, from Figure 2, we write $\Delta\sigma^{\circ}_{\mathrm{max}}(\mathrm{veg})$ corresponding to the upper-bound as,

$$\Delta\sigma^{\circ}_{\text{max}}(\text{veg}) = f(\text{veg}) + \Delta\sigma^{\circ}_{\text{max (bare)}} \tag{7}$$

where $\Delta\sigma^{\circ}_{\text{max (bare)}}$ is the maximum change in backscatter for bare soil surface and $f(\text{veg})$ is a function of vegetation index, can be linear or non-linear as mentioned previously.

From the observed data (Figure 3a), we have fitted a nonlinear wet-reference for NDVI as,

$$\Delta\sigma^{\circ}_{\text{max}}(\text{NDVI}) = -6.15 \times \text{NDVI}^2 + 0.44 \times \text{NDVI} + 7.92 \tag{8}$$

In the case of DpRVI_c (Figure 3b) we obtain the expression of $\Delta\sigma_{\text{max}}(\text{veg})$ as presented in Eq. (9),

$$\Delta\sigma^{\circ}_{\text{max}}(\text{DpRVI}_c) = -5.27 \times {\text{DpRVI}_c}^2 - 4.80 \times \text{DpRVI}_c + 9.35 \tag{9}$$

According to Wagner et al. (1999) and Zribi et al. (2008), the surface soil moisture from change detection approach can be expressed as,

$$\Theta = \frac{\Delta\sigma}{\sigma_{\text{wet}} - \sigma_{\text{dry}}} = \frac{\Delta\sigma}{\Delta\sigma^{\circ}_{\text{max}}(\text{veg})}. \tag{10}$$

Subsequently, the absolute soil moisture $\Theta_{(i,j;t:\text{veg})}$ can be calculated for each pixel (i, j) for a given time t and vegetation condition as,

$$\Theta_{(i,j;t:\text{veg})} = \frac{\Delta\sigma_{(i,j;t)}}{\Delta\sigma^{\circ}_{\text{max}}(\text{veg})}(\text{M}_{\text{v}_{\text{max}}} - \text{M}_{\text{v}_{\text{min}}}) + \text{M}_{\text{v}_{\text{min}}} \tag{11}$$

where, $\Delta\sigma_{(i,j;t)}$ represents the change in backscatter (as shown in Figure 3)

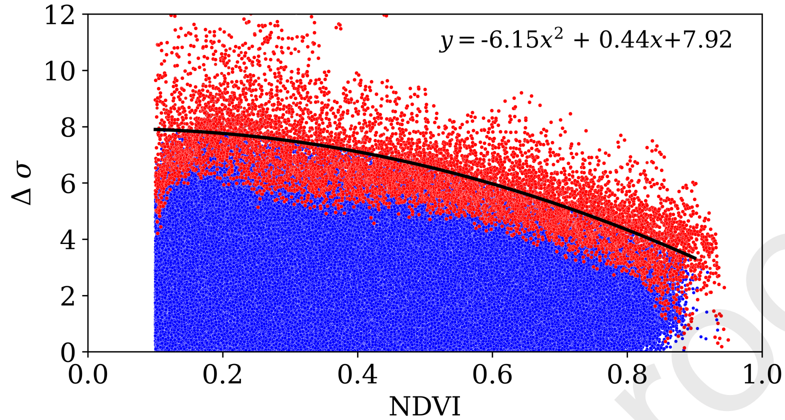

(a)

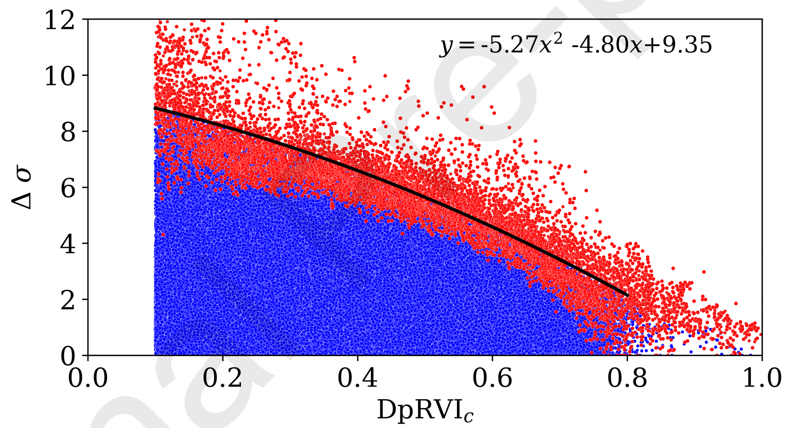

(b)

Figure 3: Change in co-pol backscatter (VV), $\Delta\sigma$(dB) as a function of (a) NDVI and (b) DpRVI_c over entire study area (TxSON) during March 2015 to August 2019. The solid line corresponds the regression line of upper 2 % of $\Delta\sigma$ (red points) for each value of vegetation index.

of pixel indexed by (i, j) at time t. $\Delta\sigma^{\circ}_{\mathrm{max}}(\mathrm{veg})$ can be calculated from Eq. (8) and Eq. (9) for NDVI and DpRVI_c respectively. $\mathrm{M}_{\mathrm{v_{max}}}$, $\mathrm{M}_{\mathrm{v_{min}}}$ are soil moisture values corresponding to field capacity and wilting point for that specific pixel. A detailed workflow of the proposed methodology is shown in

Figure 4.

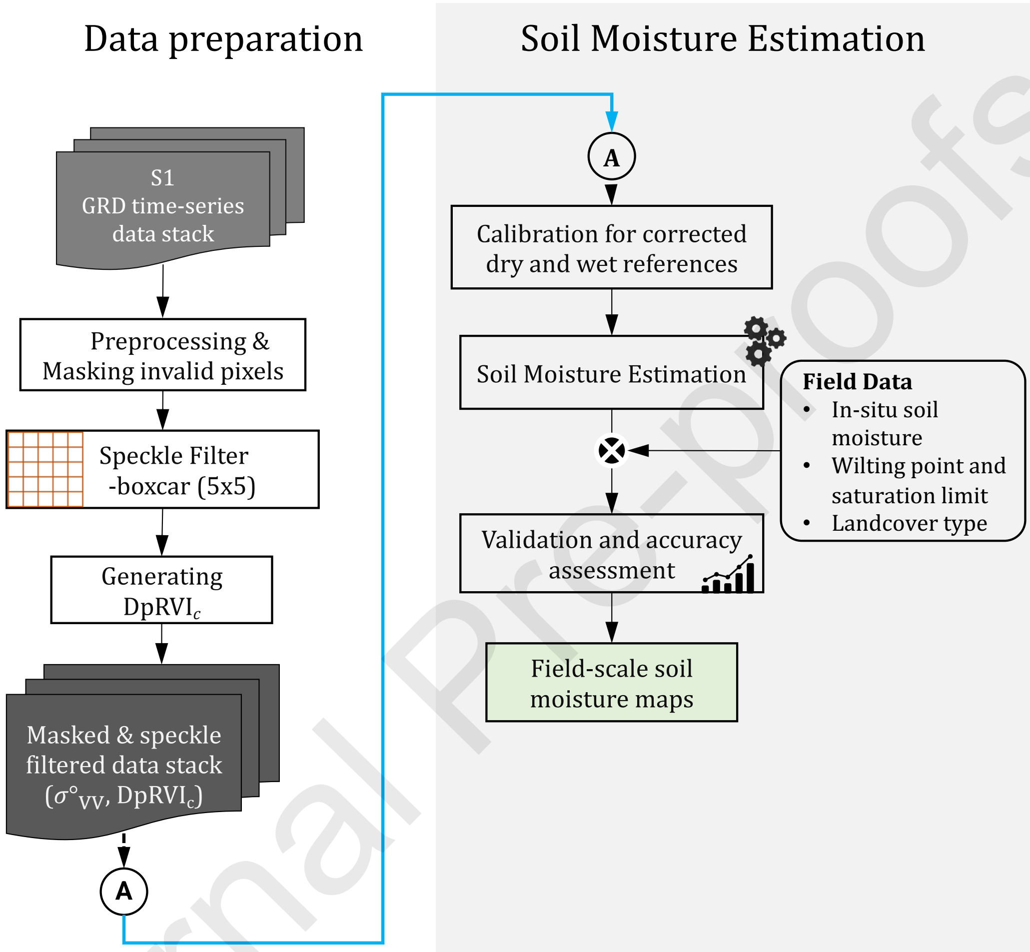

Figure 4: The schematic workflow of the proposed methodology for field-scale soil moisture estimation.

4. Results and discussion

In this section, we analyze the performance of the proposed approach with NDVI and DpRVI$_c$ over croplands and shrublands. We assessed the agreement between the estimated and in-situ soil moisture values quantitatively using the Root Mean Square Error (RMSE) (Eq. (12)) and Pearson correlation coefficient r (Eq. (13)). Results from individual sample stations are presented in Appendix A.

$$\mathrm{RMSE} = \sqrt{\sum_{i=1}^{n} \frac{(x_i - y_i)^2}{n}} \tag{12}$$

where, $x_1,\ x_2, ...,\ x_n$ are in-situ soil moisture values, $y_1,\ y_2, ...,\ y_n$ are estimated soil moisture values, and n is the number of observations.

$$r = \frac{\sum_{i=1}^{n}(x_i - \overline{x})(y_i - \overline{y})}{\sqrt{\sum_{i=1}^{n}(x_i - \overline{x})^2}\sqrt{\sum_{i=1}^{n}(y_i - \overline{y})^2}} \tag{13}$$

where, $x_1,\ x_2, ...,\ x_n$ are in-situ soil moisture values, $\overline{x}$ is the mean in-situ soil moisture, $y_1,\ y_2, ...,\ y_n$ are estimated soil moisture values, $\overline{y}$ is the mean estimated soil moisture, and n is the number of observations.

4.1. Croplands

We have considered seven soil moisture stations in the croplands for the analysis. The results obtained from NDVI and DpRVI$_c$ with Sentinel-1 data are presented in Figure 5. The accuracy metrics r and RMSE for NDVI are 0.814 and $0.076\,\mathrm{m^3\,m^{-3}}$ respectively, whereas for DpRVI$_c$ we get $r = 0.851$ and RMSE $= 0.055\,\mathrm{m^3\,m^{-3}}$. We observe a better accuracy of estimated soil moisture using DpRVI$_c$ than NDVI. Further, one can observe from the scatter plots that in the case of NDVI, a majority of the estimates are below the 1:1 line. This underestimation of soil moisture might be because of saturation of NDVI for denser canopies (Asrar et al., 1984; Hatfield et al., 1985; Sellers, 1985). In contrast, the penetration capabilities of SAR can be helpful in such scenarios to quantify the vegetation content. Moreover, as shown in previous studies (Bhogapurapu et al., 2021a), the sensitivity of the co-pol purity parameter, m_c towards vegetation growth could be a possible explanation for the better accuracy with DpRVI_c.

Temporal evolution of measured and estimated soil moisture from NDVI and DpRVI_c is presented in Figure 6. The temporal analysis revealed an underestimation when using NDVI during the high soil moisture condition. For example, the mean in-situ soil moisture during March 2015 is $0.223\,\mathrm{m^3\,m^{-3}}$ (corresponds to the mean value from seven in-situ stations), and the estimated value with NDVI is $0.164\,\mathrm{m^3\,m^{-3}}$. Whereas, in the case of DpRVI_c, the estimated mean value is $0.225\,\mathrm{m^3\,m^{-3}}$. We observed similar results for April 2016, June 2017, and January 2018. However, most of the crop fields are at early crop growth during dry periods. As a result, we observe an overestimation of soil moisture with DpRVI_c compared to NDVI. This might be due to the surface roughness effect on DpRVI_c during the early crop growth stages. Nevertheless, the estimated soil moisture values for all seven stations are in good agreement with in-situ measurements with an overall RMSE of $0.055\,\mathrm{m^3\,m^{-3}}$ in case of DpRVI_c.

4.2. Shrubland

The analysis for shrublands consists of data from 27 stations. Vegetation in these shrublands includes woody plants (Ashe juniper and honey mesquite) and a mixture of short and mid-height grasses (grama, switchgrass, bluestem, curlymesquite) (Caldwell et al., 2019).

Figure 7 shows the correlation plots between measured and estimated soil moisture for 27 stations in shrublands. We obtain an RMSE of $0.066\,\mathrm{m^3\,m^{-3}}$

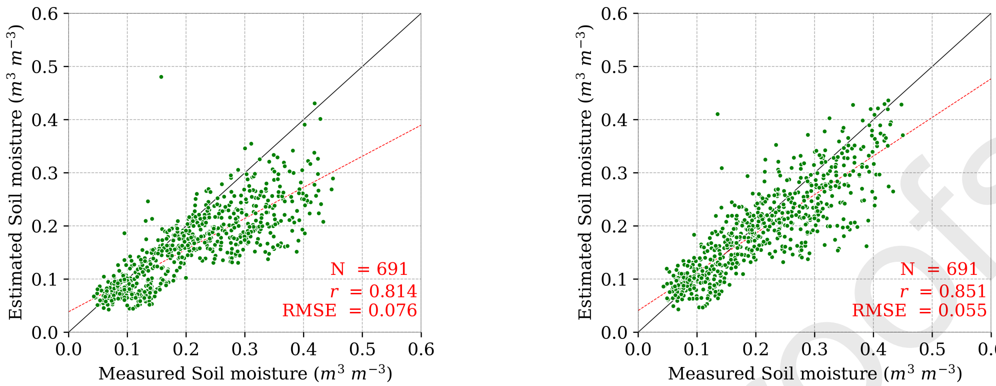

(a) (b)

Figure 5: Correlation plots between observed and retrieved soil moisture for cropland (a) using NDVI (b) using DpRVI$_c$.

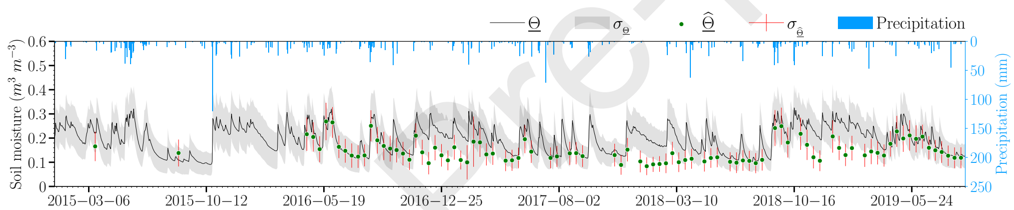

(a)

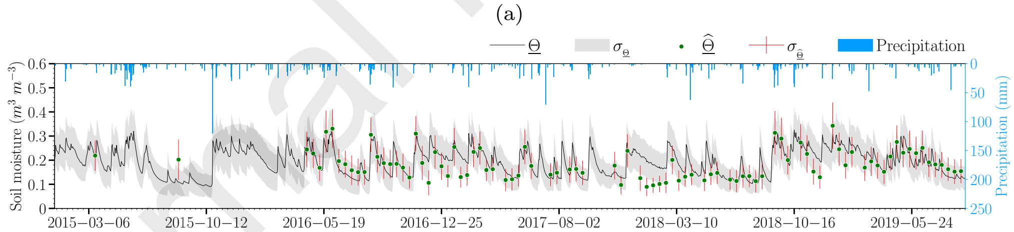

(b)

Figure 6: Temporal evolution of observed and retrieved soil moisture over croplands (a) using NDVI (b) using DpRVI$_c$ for seven stations, where, $\underline{\Theta}$: mean observed soil moisture, $\sigma_{\underline{\Theta}}$: standard deviation of observed soil moisture, $\widehat{\underline{\Theta}}$: mean retrieved soil moisture, $\sigma_{\widehat{\underline{\Theta}}}$: standard deviation of retrieved soil moisture.

with NDVI and $0.048\,\mathrm{m^3\,m^{-3}}$ with DpRVI$_c$ with a high Pearson correlation $r \geq 0.64$. We observe a better accuracy of soil moisture estimates with

DpRVI$_c$ than NDVI. Similar to the results of croplands, we witness a high underestimation of soil moisture with NDVI. This underestimation of soil moisture might be because of the saturation of NDVI for denser vegetation canopies and the nature of logarithmic relation between soil moisture and SAR signal (Zribi et al., 2020). Therefore, the penetration capabilities of SAR can be an advantage over optical data in such scenarios to quantify the vegetation content. Moreover, as shown in previous studies (Bhogapurapu et al., 2021a), the sensitivity of co-pol purity parameter m_c towards vegetation growth could be a possible explanation for the better accuracy with DpRVI$_c$.

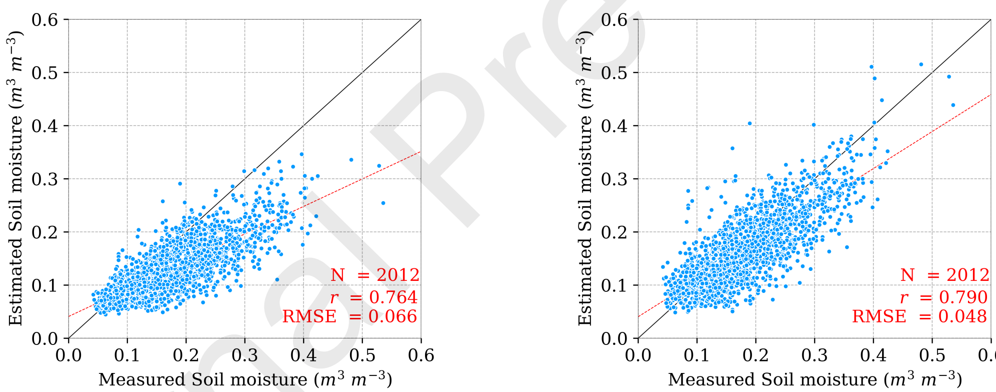

(a) (b)

Figure 7: Correlation plots between observed and retrieved soil moisture for shrubland (a) using NDVI (b) using DpRVI$_c$.

Figure 8 presents the temporal evolution of measured and estimated soil moisture from NDVI and DpRVI$_c$ over shrublands. The analysis of temporal dynamics revealed an underestimation during high soil moisture scenarios with NDVI. For example, mean in-situ soil moisture during March 2015 is $0.217\,\mathrm{m^3\,m^{-3}}$ (corresponds to the mean value from twenty-seven in-situ stations), and the estimated value with NDVI is $0.161\,\mathrm{m^3\,m^{-3}}$. In contrast, the estimates using DpRVI$_c$ are in good agreement with the in-situ measurements. However, during dry periods, soil moisture estimates from DpRVI$_c$ are marginally overestimated. This overestimation might be due to the surface roughness effect on DpRVI$_c$ because of sparse vegetation conditions and relatively drier canopy. Nevertheless, the estimated soil moisture values for all twenty-seven stations are in good agreement with in-situ measurements with overall RMSE of $0.048\,\mathrm{m^3\,m^{-3}}$ in case of DpRVI$_c$.

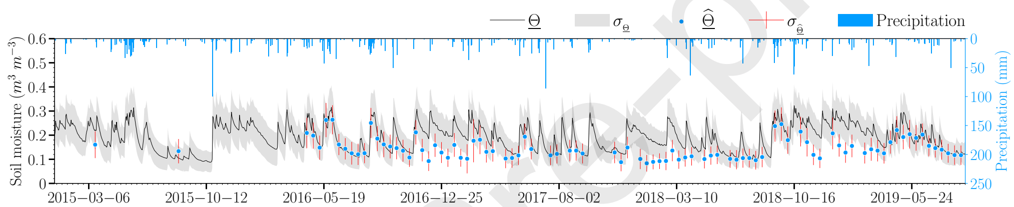

(a)

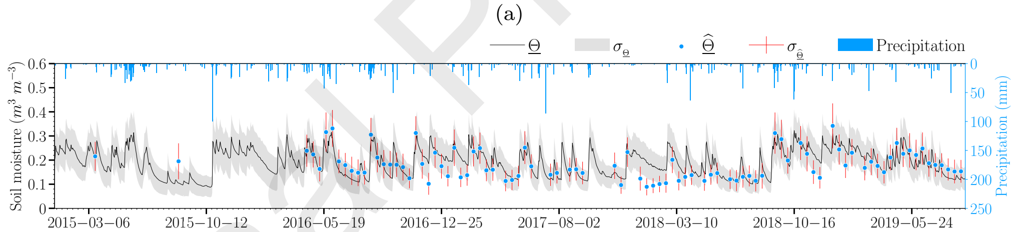

(b)

Figure 8: Temporal evolution of observed and retrieved soil moisture over shrub land for 27 stations (a) with NDVI (b) DpRVI$_c$, where, $\underline{\Theta}$: mean observed soil moisture, $\sigma_{\underline{\Theta}}$: standard deviation of observed soil moisture, $\widehat{\underline{\Theta}}$: mean retrieved soil moisture, $\sigma_{\widehat{\underline{\Theta}}}$: standard deviation of retrieved soil moisture.

We presented the spatiotemporal soil moisture maps derived using the DpRVI$_c$ in Figure 9. The maps correspond to each year's dry and wet periods from 2016 to 2019. From the observed in-situ data, the dry periods corresponds to late April and early May month of the corresponding year.

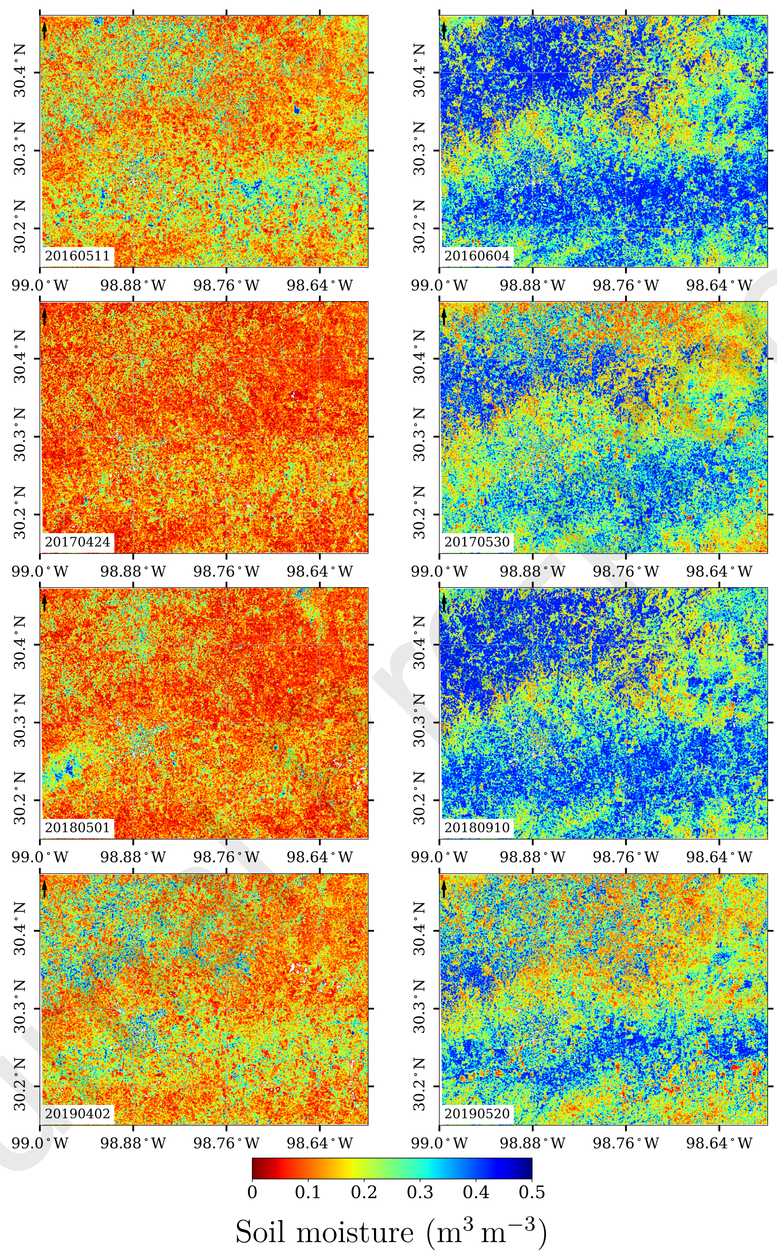

Figure 9: Soil moisture maps derived using DpRVI$_c$ from Sentinel-1 GRD SAR data over the test site. The dry and wet periods of each year (2016-2019) are shown in rows one and two.

According to the Texas Water Development board Reports TWDB (2012), rainfall events occur from late May to early June and early September. Therefore, from Figure 9 we observe high soil moisture values over the entire study area during these periods. Further, these dry and wet trends are also supported by the in-situ soil moisture stations (Figures 6 and 8).

Pedernales River basin spans the study area from east to west at 30.2°N latitude. Croplands dominate either side of the river, and further, due to the elevation profile of the terrain, we observe relatively higher soil moisture in this area. In contrast, we witness lower soil moisture values in the area at higher elevations and slopes (e.g., at 30.3°N latitude). These observations are in good agreement with the in-situ station data. Further, the temporal dynamics of estimated soil moisture agree well with precipitation data. The correlation and temporal analysis demonstrated that SAR-derived vegetation indices could correct vegetation effects when estimating soil moisture. There is a good agreement between the in-situ measured and the estimated soil moisture for various vegetation conditions.

5. Conclusion

This paper proposes removing the vegetation effect to estimate soil moisture using a change detection approach. The proposed method uses a SAR-derived vegetation index (DpRVI_c) for Dual-pol Ground Range Detected (GRD) SAR data. Furthermore, this study presented a comparative analysis with the often-used Normalized Difference Vegetation Index (NDVI). With this proposed approach, ancillary sources for vegetation data, such as the optical-based NDVI, are not required to estimate soil moisture for vegetated soils. Optical-based methods are also prone to data gaps due to cloud cover and saturation of the signal at peak biomass. One should note that as the GRD dual-pol modes do not retain the phase information, one cannot utilize scattering decomposition techniques to separate the influence of vegetation on soil backscatter.

We evaluated the performance of the proposed technique in estimating soil moisture for shrubland and croplands using over four years of data from the Texas Soil Observation Network in the United States. The SAR-derived DpRVI_c achieved a good agreement between station measured and estimated soil moisture using Sentinel-1 GRD SAR data. The RMSE values are $0.048\,\mathrm{m}^3\,\mathrm{m}^{-3}$ and $0.055\,\mathrm{m}^3\,\mathrm{m}^{-3}$ for shrub and croplands, respectively, along with a high Pearson correlation coefficient $r \geq 0.79$.

However, the vegetation structure and water content impact the backscatter coefficient, which NDVI does not capture. Therefore additional information regarding the structure may improve the soil moisture estimates using SAR-derived vegetation indices. Besides, one can enhance the results with the availability of high temporal datasets. These results provide new insights into using dual-pol GRD SAR data to retrieve soil moisture for vegetated soils, an important finding for future missions like NISAR and ROSE-L. However, weather events such as rainfall can affect the proposed SAR-based vegetation descriptor at the time of image acquisition. The approach developed using these C-band data can be transferred and tested for other frequency bands, although saturation at high biomass might be expected for higher frequencies. In the L-band sensors, such as the one proposed for the upcoming NISAR and ROSE-L missions, one could utilize longer wavelengths to characterize scattering as canopy biomass accumulates. Finally, the results could be more robust if a multi-frequency approach is considered, such as exploiting high-frequency SAR for vegetation parameter estimation and low-frequencies for soil moisture estimation.

Appendix A. Estimated soil moisture from individual stations

This appendix presents details of individual sample stations over cropland and shrubland using DpRVI$_c$.

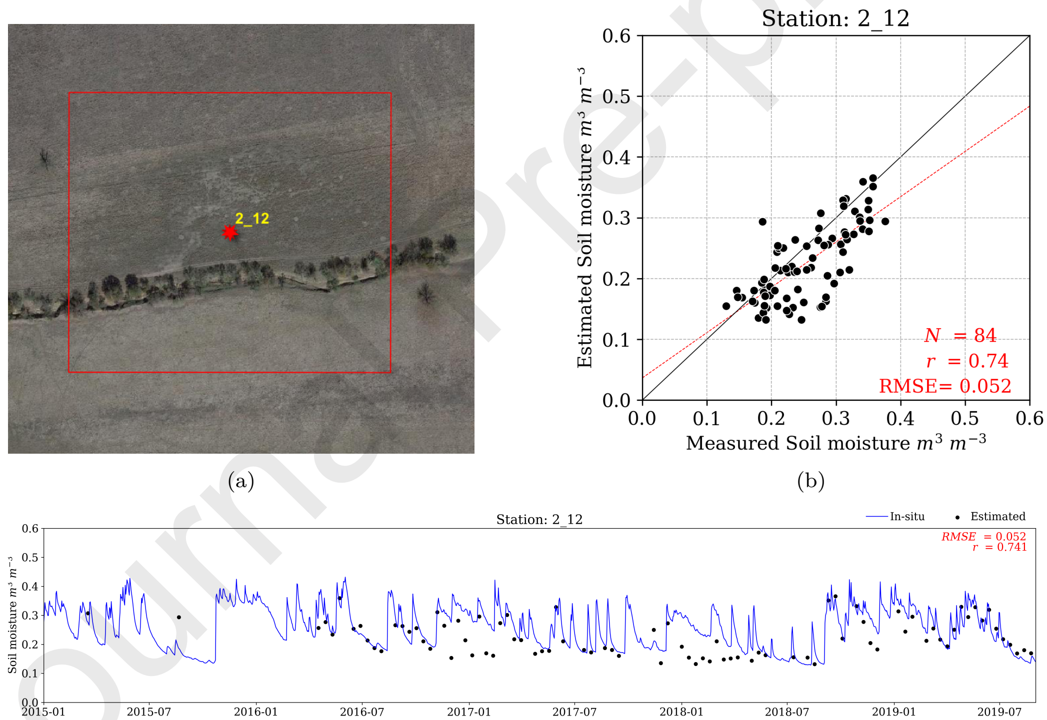

(a) (b) (c)

Figure A.10: Details of a sample station over cropland (2_12) (a) station location overlaid on an optical image with a buffer polygon with side length of 250 m (b) scatter plot of measured and estimated soil moisture (c) temporal variation of measured and estimated soil moisture

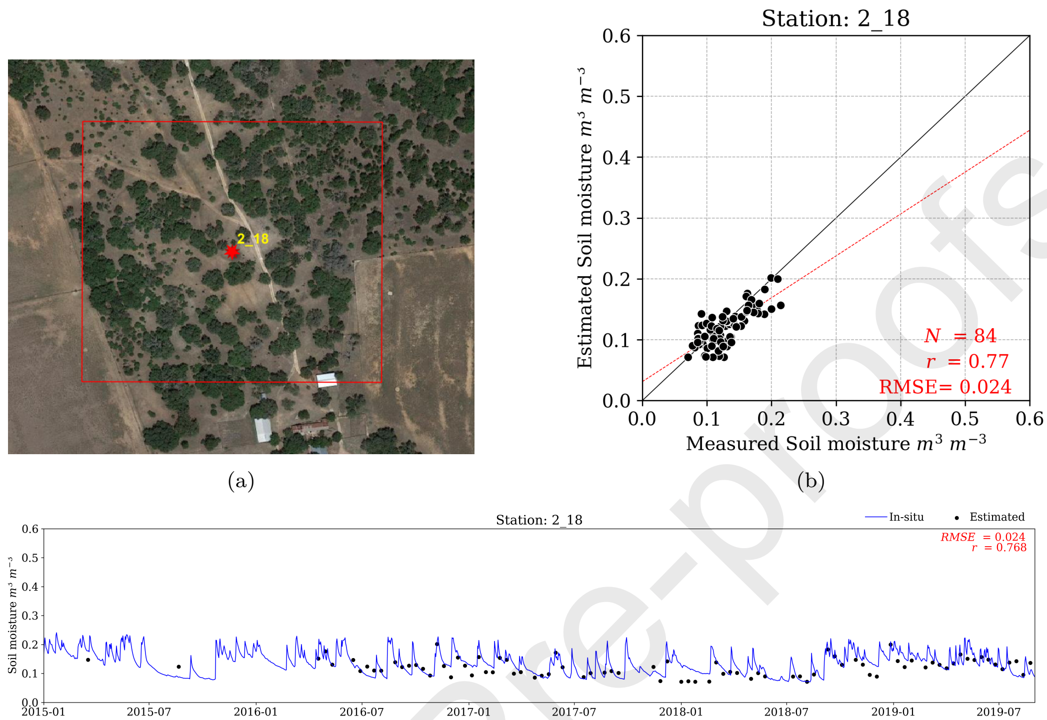

(c)

Figure A.11: Details of a sample station over shrubland (2_18) (a) station location overlaid on an optical image with a buffer polygon with side length of 250 m (b) scatter plot of measured and estimated soil moisture (c) temporal variation of measured and estimated soil moisture

Disclosures

No potential conflict of interest was reported by the authors.

Acknowledgment

The authors are grateful to the TxSON science team for providing ground truth information. The authors would like to thank the Google Earth Engine team for providing the free SAR data processing platform. Authors also acknowledge the GEO-AWS Earth Observation Cloud Credits Program, which supported the computation with Sentinel-1 on AWS cloud platform through the project: "AWS4AgriSAR-Crop inventory mapping from SAR data on a cloud computing platform", and formed the testbed for processing pipelines. Narayanarao Bhogapurapu, and Subhadip Dey would like to acknowledge the support of MHRD, Govt. of India, towards their doctoral research. The authors are thankful for the overleaf (`https://overleaf.com/`) team for providing the free online latex editing platform.

References

Asner, G. P., Scurlock, J. M., A. Hicke, J., 2003. Global synthesis of leaf area index observations: implications for ecological and remote sensing studies. Global Ecology and Biogeography 12 (3), 191–205.

Asrar, G., Fuchs, M., Kanemasu, E., Hatfield, J., 1984. Estimating absorbed photosynthetic radiation and leaf area index from spectral reflectance in wheat 1. Agronomy journal 76 (2), 300–306.

Attarzadeh, R., Amini, J., Notarnicola, C., Greifeneder, F., 2018. Synergetic use of Sentinel-1 and Sentinel-2 data for soil moisture mapping at plot scale. Remote Sensing 10 (8), 1285.

Baghdadi, N., Holah, N., Zribi, M., 2006. Soil moisture estimation using multi-incidence and multi-polarization ASAR data. International Journal of Remote Sensing 27 (10), 1907–1920.

Baghdadi, N. N., El Hajj, M., Zribi, M., Fayad, I., 2015. Coupling SAR C-band and optical data for soil moisture and leaf area index retrieval over irrigated grasslands. IEEE Journal of Selected Topics in Applied Earth Observations and Remote Sensing 9 (3), 1229–1243.

Balenzano, A., Mattia, F., Satalino, G., Davidson, M. W., 2010. Dense temporal series of C-and L-band SAR data for soil moisture retrieval over agricultural crops. IEEE Journal of Selected Topics in Applied Earth Observations and Remote Sensing 4 (2), 439–450.

Balenzano, A., Mattia, F., Satalino, G., Lovergine, F. P., Palmisano, D., Peng, J., Marzahn, P., Wegmüller, U., Cartus, O., Dabrowska-Zielińska, K., et al., 2021. Sentinel-1 soil moisture at 1 km resolution: a validation study. Remote Sensing of Environment 263, 112554.

Bao, Y., Lin, L., Wu, S., Deng, K. A. K., Petropoulos, G. P., 2018. Surface soil moisture retrievals over partially vegetated areas from the synergy of Sentinel-1 and Landsat 8 data using a modified water-cloud model. International journal of applied earth observation and geoinformation 72, 76–85.

Bauer-Marschallinger, B., Freeman, V., Cao, S., Paulik, C., Schaufler, S., Stachl, T., Modanesi, S., Massari, C., Ciabatta, L., Brocca, L., et al., 2018. Toward global soil moisture monitoring with Sentinel-1: Harnessing assets and overcoming obstacles. IEEE Transactions on Geoscience and Remote Sensing 57 (1), 520–539.

Bhogapurapu, N., Dey, S., Bhattacharya, A., Mandal, D., Lopez-Sanchez, J. M., McNairn, H., López-Martínez, C., Rao, Y. S., 2021a. Dual-polarimetric descriptors from Sentinel-1 GRD SAR data for crop growth assessment. ISPRS Journal of Photogrammetry and Remote Sensing 178, 20–35.

Bhogapurapu, N., Dey, S., Bhattacharya, A., Rao, Y., 2021b. Soil moisture estimation using simulated nisar dual polarimetric grd product over croplands. In: 2021 7th Asia-Pacific Conference on Synthetic Aperture Radar (APSAR). IEEE, pp. 1–6.

Bhogapurapu, N., Dey, S., Mandal, D., Bhattacharya, A., Karthikeyan, L., McNairn, H., Rao, Y., 2022. Soil moisture retrieval over croplands using dual-pol l-band grd sar data. Remote Sensing of Environment 271, 112900.

Bhogapurapu, N., Dey, S., Mandal, D., Bhattacharya, A., Rao, Y., 2021c. Polsar tools: A qgis plugin for generating sar descriptors. Journal of Open Source Software 6 (60), 2970.

Bhogapurapu, N., Mandal, D., Rao, Y., Bhattacharya, A., 2020a. Soil Moisture Estimation for Wheat Crop Using Dual-Pol L-Band SAR Data. In: 2020 IEEE India Geoscience and Remote Sensing Symposium (InGARSS). IEEE, pp. 33–36.

Bhogapurapu, N., Mandal, D., Rao, Y., Bhattacharya, A., 2020b. Soil Moisture Retrieval Using SAR Derived Vegetation Descriptors in Water Cloud Model. In: IGARSS 2020-2020 IEEE International Geoscience and Remote Sensing Symposium. IEEE, pp. 4696–4699.

Caldwell, T. G., Bongiovanni, T., Cosh, M. H., Jackson, T. J., Colliander, A., Abolt, C. J., Casteel, R., Larson, T., Scanlon, B. R., Young, M. H., 2019. The texas soil observation network: A comprehensive soil moisture dataset for remote sensing and land surface model validation. Vadose Zone Journal 18 (1), 1–20.

Champagne, C., Berg, A., McNairn, H., Drewitt, G., Huffman, T., 2012. Evaluation of soil moisture extremes for agricultural productivity in the Canadian prairies. Agricultural and forest meteorology 165, 1–11.

Chen, P.-Y., Fedosejevs, G., Tiscareno-Lopez, M., Arnold, J. G., 2006. Assessment of MODIS-EVI, MODIS-NDVI and VEGETATION-NDVI composite data using agricultural measurements: An example at corn fields in western Mexico. Environmental monitoring and assessment 119 (1), 69–82.

Cloude, S., 2009. Polarisation: applications in remote sensing. Oxford University Press, Oxford.

Della Vecchia, A., Ferrazzoli, P., Guerriero, L., Ninivaggi, L., Strozzi, T., Wegmuller, U., 2008. Observing and modeling multifrequency scattering of maize during the whole growth cycle. IEEE Transactions on Geoscience and Remote Sensing 46 (11), 3709–3718.

Dey, S., Bhattacharya, A., Ratha, D., Mandal, D., McNairn, H., Lopez-Sanchez, J. M., Rao, Y., 2020a. Novel clustering schemes for full and compact polarimetric sar data: An application for rice phenology characterization. ISPRS Journal of Photogrammetry and Remote Sensing 169, 135–151.

Dey, S., Bhogapurapu, N., Bhattacharya, A., Mandal, D., Lopez-Sanchez, J. M., McNairn, H., Frery, A. C., 2021a. Rice phenology mapping using novel target characterization parameters from polarimetric sar data. International Journal of Remote Sensing 42 (14), 5519–5543.

Dey, S., Chaudhuri, U., Bhogapurapu, N., Lopez-Sanchez, J. M., Banerjee, B., Bhattacharya, A., Mandal, D., Rao, Y. S., 2021b. Synergistic use of tandem-x and landsat-8 data for crop-type classification and monitoring. IEEE Journal of Selected Topics in Applied Earth Observations and Remote Sensing 14, 8744–8760.

Dey, S., Chaudhuri, U., Mandal, D., Bhattacharya, A., Banerjee, B., McNairn, H., 2020b. Biophynet: A regression network for joint estimation of plant area index and wet biomass from sar data. IEEE Geoscience and Remote Sensing Letters 18 (10), 1701–1705.

Dey, S., Mandal, D., Robertson, L. D., Banerjee, B., Kumar, V., McNairn, H., Bhattacharya, A., Rao, Y., 2020c. In-season crop classification using elements of the kennaugh matrix derived from polarimetric radarsat-2 sar data. International Journal of Applied Earth Observation and Geoinformation 88, 102059.

Dubois, P. C., Van Zyl, J., Engman, T., 1995. Measuring soil moisture with imaging radars. IEEE transactions on geoscience and remote sensing 33 (4), 915–926.

El Hajj, M., Baghdadi, N., Zribi, M., Bazzi, H., 2017. Synergic use of Sentinel-1 and Sentinel-2 images for operational soil moisture mapping at high spatial resolution over agricultural areas. Remote Sensing 9 (12), 1292.

Fung, A. K., Li, Z., Chen, K.-S., 1992. Backscattering from a randomly rough dielectric surface. IEEE Transactions on Geoscience and remote sensing 30 (2), 356–369.

Gao, Q., Zribi, M., Escorihuela, M. J., Baghdadi, N., 2017. Synergetic use of sentinel-1 and sentinel-2 data for soil moisture mapping at 100 m resolution. Sensors 17 (9), 1966.

Hajnsek, I., et al., 2009. Potential of estimating soil moisture under vegetation cover by means of PolSAR. IEEE Trans. Geosci. Remote Sens. 47 (2), 442–454.

Hatfield, J., Kanemasu, E., Asrar, G., Jackson, R., Pinter Jr, P., Reginato, R., Idso, S., 1985. Leaf-area estimates from spectral measurements over various planting dates of wheat. International Journal of Remote Sensing 6 (1), 167–175.

Hobbs, T. J., 1995. The use of NOAA-AVHRR NDVI data to assess herbage production in the arid rangelands of Central Australia. International Journal of Remote Sensing 16 (7), 1289–1302.

Homayouni, S., McNairn, H., Hosseini, M., Jiao, X., Powers, J., 2019. Quad and compact multitemporal C-band PolSAR observations for crop characterization and monitoring. International Journal of Applied Earth Observation and Geoinformation 74, 78–87.

Hornacek, M., Wagner, W., Sabel, D., Truong, H.-L., Snoeij, P., Hahmann, T., Diedrich, E., Doubková, M., 2012. Potential for high resolution systematic global surface soil moisture retrieval via change detection using

Sentinel-1. IEEE Journal of Selected Topics in Applied Earth Observations and Remote Sensing 5 (4), 1303–1311.

Ines, A. V., Das, N. N., Hansen, J. W., Njoku, E. G., 2013. Assimilation of remotely sensed soil moisture and vegetation with a crop simulation model for maize yield prediction. Remote Sensing of Environment 138, 149–164.

Jagdhuber, T., Hajnsek, I., Bronstert, A., Papathanassiou, K. P., 2012. Soil moisture estimation under low vegetation cover using a multi-angular polarimetric decomposition. IEEE Transactions on Geoscience and Remote Sensing 51 (4), 2201–2215.

Karthikeyan, L., Chawla, I., Mishra, A. K., 2020. A review of remote sensing applications in agriculture for food security: Crop growth and yield, irrigation, and crop losses. Journal of Hydrology 586, 124905.

Karthikeyan, L., Pan, M., Wanders, N., Kumar, D. N., Wood, E. F., 2017. Four decades of microwave satellite soil moisture observations: Part 1. a review of retrieval algorithms. Advances in Water Resources 109, 106–120.

Kim, S.-B., Moghaddam, M., Tsang, L., Burgin, M., Xu, X., Njoku, E. G., 2013. Models of L-band radar backscattering coefficients over global terrain for soil moisture retrieval. IEEE Transactions on Geoscience and Remote Sensing 52 (2), 1381–1396.

Li, J., Wang, S., 2018. Using SAR-Derived Vegetation Descriptors in a Water Cloud Model to Improve Soil Moisture Retrieval. Remote Sensing 10 (9), 1370.

Liu, J., Pattey, E., Jégo, G., 2012. Assessment of vegetation indices for regional crop green LAI estimation from Landsat images over multiple growing seasons. Remote Sensing of Environment 123, 347–358.

Ma, C., Li, X., McCabe, M. F., 2020. Retrieval of High-Resolution Soil Moisture through Combination of Sentinel-1 and Sentinel-2 Data. Remote Sensing 12 (14), 2303.

Mandal, D., Kumar, V., Ratha, D., Dey, S., Bhattacharya, A., Lopez-Sanchez, J. M., McNairn, H., Rao, Y. S., 2020. Dual polarimetric radar vegetation index for crop growth monitoring using Sentinel-1 SAR data. Remote Sensing of Environment 247, 111954.

Martínez-Fernández, J., González-Zamora, A., Sánchez, N., Gumuzzio, A., Herrero-Jiménez, C., 2016. Satellite soil moisture for agricultural drought monitoring: Assessment of the SMOS derived Soil Water Deficit Index. Remote Sensing of Environment 177, 277–286.

Massari, C., Camici, S., Ciabatta, L., Brocca, L., 2018. Exploiting satellite-based surface soil moisture for flood forecasting in the Mediterranean area: State update versus rainfall correction. Remote Sensing 10 (2), 292.

Millard, K., Richardson, M., 2018. Quantifying the relative contributions of vegetation and soil moisture conditions to polarimetric C-Band SAR response in a temperate peatland. Remote sensing of environment 206, 123–138.

Mishra, A., Vu, T., Veettil, A. V., Entekhabi, D., 2017. Drought monitoring with soil moisture active passive (SMAP) measurements. Journal of Hydrology 552, 620–632.

Mutanga, O., Skidmore, A. K., 2004. Narrow band vegetation indices overcome the saturation problem in biomass estimation. International journal of remote sensing 25 (19), 3999–4014.

Oh, Y., Sarabandi, K., Ulaby, F. T., et al., 1992. An empirical model and an inversion technique for radar scattering from bare soil surfaces. IEEE transactions on Geoscience and Remote Sensing 30 (2), 370–381.

Ouellette, J. D., Johnson, J. T., Balenzano, A., Mattia, F., Satalino, G., Kim, S.-B., Dunbar, R. S., Colliander, A., Cosh, M. H., Caldwell, T. G., et al., 2017. A time-series approach to estimating soil moisture from vegetated surfaces using L-band radar backscatter. IEEE transactions on geoscience and remote sensing 55 (6), 3186–3193.

Paloscia, S., Pettinato, S., Santi, E., Notarnicola, C., Pasolli, L., Reppucci, A., 2013. Soil moisture mapping using Sentinel-1 images: Algorithm and preliminary validation. Remote Sensing of Environment 134, 234–248.

Pauwels, V. R., De Lannoy, G. J., 2006. Improvement of modeled soil wetness conditions and turbulent fluxes through the assimilation of observed discharge. Journal of hydrometeorology 7 (3), 458–477.

Periasamy, S., 2018. Significance of dual polarimetric synthetic aperture radar in biomass retrieval: An attempt on Sentinel-1. Remote Sensing of Environment 217, 537–549.

Rousel, J., Haas, R., Schell, J., Deering, D., 1973. Monitoring vegetation systems in the great plains with erts. In: Proceedings of the Third Earth Resources Technology Satellite—1 Symposium; NASA SP-351. pp. 309–317.

Scipal, K., Drusch, M., Wagner, W., 2008. Assimilation of a ERS scatterometer derived soil moisture index in the ECMWF numerical weather prediction system. Advances in water resources 31 (8), 1101–1112.

Sellers, P. J., 1985. Canopy reflectance, photosynthesis and transpiration. International journal of remote sensing 6 (8), 1335–1372.

Seneviratne, S. I., Corti, T., Davin, E. L., Hirschi, M., Jaeger, E. B., Lehner, I., Orlowsky, B., Teuling, A. J., 2010. Investigating soil moisture–climate interactions in a changing climate: A review. Earth-Science Reviews 99 (3-4), 125–161.

Shi, J., Wang, J., Hsu, A. Y., O'Neill, P. E., Engman, E. T., 1997. Estimation of bare surface soil moisture and surface roughness parameter using L-band SAR image data. IEEE Transactions on Geoscience and Remote Sensing 35 (5), 1254–1266.

Trudel, M., Charbonneau, F., Leconte, R., 2012. Using RADARSAT-2 polarimetric and ENVISAT-ASAR dual-polarization data for estimating soil moisture over agricultural fields. Canadian Journal of Remote Sensing 38 (4), 514–527.

TWDB, 2012. Climate of Texas. https://www.twdb.texas.gov/publications/state_water_plan/2012/

Ulaby, F., 1974. Radar measurement of soil moisture content. IEEE Transactions on Antennas and propagation 22 (2), 257–265.

Ulaby, F. T., 1982. Microwave remote sensing active and passive. Rader remote sensing and surface scattering and emission theory, 848–902.

Ulaby, F. T., Batlivala, P. P., Dobson, M. C., 1978. Microwave backscatter dependence on surface roughness, soil moisture, and soil texture: Part I-bare soil. IEEE Transactions on Geoscience Electronics 16 (4), 286–295.

Vreugdenhil, M., Wagner, W., Bauer-Marschallinger, B., Pfeil, I., Teubner, I., Rüdiger, C., Strauss, P., 2018. Sensitivity of Sentinel-1 backscatter to vegetation dynamics: An Austrian case study. Remote Sensing 10 (9), 1396.

Wagner, W., Noll, J., Borgeaud, M., Rott, H., 1999. Monitoring soil moisture over the Canadian Prairies with the ERS scatterometer. IEEE Transactions on Geoscience and Remote Sensing 37 (1), 206–216.

Wanders, N., Karssenberg, D., Roo, A. d., De Jong, S., Bierkens, M., 2014. The suitability of remotely sensed soil moisture for improving operational flood forecasting. Hydrology and Earth System Sciences 18 (6), 2343–2357.

Zribi, M., André, C., Decharme, B., 2008. A method for soil moisture estimation in western africa based on the ers scatterometer. IEEE Transactions on Geoscience and Remote Sensing 46 (2), 438–448.

Zribi, M., Foucras, M., Baghdadi, N., Demarty, J., Muddu, S., 2020. A new reflectivity index for the retrieval of surface soil moisture from radar data. IEEE Journal of Selected Topics in Applied Earth Observations and Remote Sensing 14, 818–826.